NASA/TM – 2024-219027/ Vol. 13

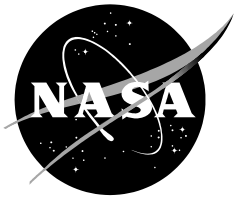

PACE Technical Report Series, Volume 13

Editors:
Ivona Cetinić, GESTAR II/Morgan State University, Baltimore, Maryland
Charles R. McClain, retired from NASA Goddard Space Flight Center, Greenbelt, Maryland
P. Jeremy Werdell, NASA Goddard Space Flight Center, Greenbelt, Maryland

PACE OCI Calibration and Geolocation Operational Algorithm Description

Frederick S. Patt, Science Applications International Corporation, Reston, Virginia

July 2024

NASA STI Program Report Series

The NASA STI Program collects, organizes, provides for archiving, and disseminates NASA's STI. The NASA STI program provides access to the NTRS Registered and its public interface, the NASA Technical Reports Server, thus providing one of the largest collections of aeronautical and space science STI in the world. Results are published in both non-NASA channels and by NASA in the NASA STI Report Series, which includes the following report types:

- TECHNICAL PUBLICATION. Reports of completed research or a major significant phase of research that present the results of NASA Programs and include extensive data or theoretical analysis. Includes compilations of significant scientific and technical data and information deemed to be of continuing reference value. NASA counterpart of peer-reviewed formal professional papers but has less stringent limitations on manuscript length and extent of graphic presentations.

- TECHNICAL MEMORANDUM. Scientific and technical findings that are preliminary or of specialized interest, e.g., quick release reports, working papers, and bibliographies that contain minimal annotation. Does not contain extensive analysis.

- CONTRACTOR REPORT. Scientific and technical findings by NASA-sponsored contractors and grantees.

- CONFERENCE PUBLICATION. Collected papers from scientific and technical conferences, symposia, seminars, or other meetings sponsored or co-sponsored by NASA.

- SPECIAL PUBLICATION. Scientific, technical, or historical information from NASA programs, projects, and missions, often concerned with subjects having substantial public interest.

- TECHNICAL TRANSLATION. English-language translations of foreign scientific and technical material pertinent to NASA's mission.

Specialized services also include organizing and publishing research results, distributing specialized research announcements and feeds, providing information desk and personal search support, and enabling data exchange services.

For more information about the NASA STI program, see the following:

- Access the NASA STI program home page at http://www.sti.nasa.gov

- Help desk contact information:

https://www.sti.nasa.gov/sti-contact-form/ and select the "General" help request type.

NASA/ TM – 2024-219027/ Vol. 13

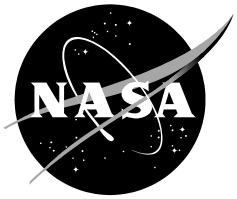

PACE Technical Report Series, Volume 13

Editors:
Ivona Cetinić, GESTAR II/Morgan State University, Baltimore, Maryland
Charles R. McClain, retired from NASA Goddard Space Flight Center, Greenbelt, Maryland
P. Jeremy Werdell, NASA Goddard Space Flight Center, Greenbelt, Maryland

PACE OCI Calibration and Geolocation Operational Algorithm Description

Frederick S. Patt, Science Applications International Corporation, Reston, Virginia

National Aeronautics and
Space Administration
Goddard Space Flight Center
Greenbelt, MD 20771-0001

July 2024

I. Contents

I. Introduction

This technical report describes the software implementation of the calibration and geolocation processing algorithms for the Ocean Color Instrument (OCI) on the Plankton, Aerosol, Cloud, ocean Ecosystem (PACE) mission. PACE was launched on February 8, 2024. The first Earth-viewing data were collected on February 25, and commissioning was completed on April 5.

All PACE science data are acquired and processed by the Science Data Segment (SDS). The first processing stages are Level 0-to-1A and Level 1A-to-1B. The calibration and geolocation processing is performed during the latter stage. The L1B products are the inputs for geophysical retrieval processing (Level 2).

This report is organized as follows. The pertinent characteristics of OCI for calibration and geolocation processing are described in Section II. Section III describes the implementation of the geolocation processing algorithms, and the calibration processing is described in Section IV. The Level 1B product format is described in Section V.

II. OCI Data Characteristics (Ref. 1)

OCI provides hyperspectral coverage from 315nm to 895nm and multispectral coverage (seven discrete wavelengths) from 940nm to 2260nm. This coverage is provided by three Focal Plane Assemblies (FPAs): Blue, Red, and SWIR. Gratings disperse the light to CCDs for the Blue and Red FPAs. The CCDs capture the light with 512 pixels in the spectral dimension (columns) and 128 pixels in the spatial dimension (rows). The spectral band-center spacing is 0.625 nm. The SWIR bands use photodiodes with spectral bandpass filters. The data characteristics for both types of FPAs are described below.

A. Hyperspectral bands

The OCI rotating telescope assembly (RTA) rotates at 5.7 Hz. The charge in the CCDs is transferred across the rows at the same rate as the image movement from the RTA rate. The result is that the charge from a given location on the Earth is accumulated via time-delay integration (TDI) and output as a single measurement via an analog-to-digital converter (ADC). Each measurement ("physical pixel") corresponds to a viewed area of 1 km along-track by 125m cross-track at nadir.

The PACE onboard storage and data downlink capacity does not allow the OCI hyperspectral data to be stored and downlinked at full resolution. The data are aggregated both spatially and spectrally before being packetized and transferred to the spacecraft data storage board (DSB). The aggregation factors are specified for different data collection modes by mode control tables stored on the instrument. The supported aggregation factors are 1, 2, 4 and 8.

The spatial data collection within each rotation of the RTA ("scan" or "spin") is specified as a series of "zones", or "views", where each zone consists of a contiguous range of pixels. A typical mode has one science view and one dark view. The spatial aggregation factor is the same for all spectral bands from both focal planes but can be set separately for each view. For baseline Earth-viewing science data collection, the spatial aggregation factor is 8, forming "science pixels" of 1x1 km at nadir. The views for baseline science are illustrated in Figure 1 (Ref. 2), which shows the nominal Earth view (scan angle range +/-56.6 degrees) and dark view. The figure also shows the pulse-per-revolution (PPR) that is the reference point for specifying

the range for each view. The view specifications and their use for geolocation processing is described in more detail in Section III.D.

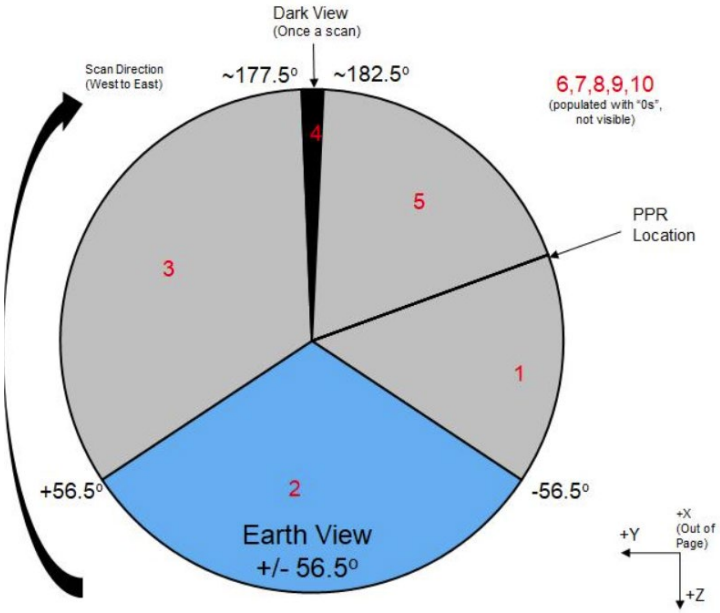

Figure 1. Data collection views for baseline science mode.

The spectral band outputs are handled by 16 "taps" per FPA, with each tap handling 32 columns from the CCD. The spectral aggregation can be set independently for each tap. In addition, taps can be enabled or disabled independently. For all but diagnostic test modes, the taps for the shortest UV (below 315 nm) and longest IR (above 897 nm) wavelengths from the Blue and Red FPAs, respectively have been disabled because the optical throughput is too low to make the outputs useful; thus there are 15 active taps for each FPA. Spectral aggregation is described in more detail in Section IV.C.

The unaggregated outputs from the ADCs are 14 bits. The output measurements are 16 bits; in order to maintain full dynamic range, for combined aggregation factors (spatial x spectral) greater than 4 the summed outputs are bit-shifted for all views except the dark view (Ref. 2).

B. SWIR bands

OCI has nine SWIR channels covering seven spectral bands with nominal center wavelengths 940, 1038, 1250, 1378, 1615, 2130 and 2260 nm. Two of the bands (1250 and 1615) have standard-gain and high-gain channels. Each channel has from two to eight detectors; the measurements from the detectors for a channel are combined via TDI to generate a single output per channel and pixel. The individual detector samples are 16 bits, and the outputs are 20 bits to preserve both radiometric range and stability. The detector sampling does result in along-scan shifts; the data are pixel-shifted during L1A processing to bring all channels into registration with the hyperspectral bands.

The SWIR bands have fixed spatial resolution equivalent to the CCD spatial aggregation factor of 8, or 1x1 km at nadir. The views within a scan are identical to those of the hyperspectral bands.

The SWIR band electronics design results in an extended, low-level response to bright sources that exceeds the radiometric accuracy requirement (Ref. 3). The correction for this effect is applied during calibration processing as described in Section IV.D.7.

III. Geolocation Processing

The geolocation processing determines the viewed locations for every OCI measurement, along with related angles used for downstream processing. The algorithms and their implementation are described in the sections below as follows: reference frame definitions; inputs to the processing; the look-up table (LUT); processing of the navigation (attitude and ephemeris) data; calculation of OCI viewing geometry; ellipsoid geolocation; terrain correction; and quality flags.

A. Reference frame definitions and transformations

The following coordinate reference frames and transformations are used in the OCI geolocation processing. Unless otherwise stated, all transformations are 3x3 orthonormal matrices.

1. J2000 inertial (Ref. 4)

The J2000 inertial frame is a standard reference frame used in many applications. It is defined as follows: X axis by the vernal equinox (intersection of the planes of the Earth mean equator and Earth orbit, or ecliptic) at epoch 12:00 UTC on January 1, 2000; Z axis in the direction of the Earth mean north pole at the epoch; Y axis completes the right-handed triad.

2. Earth-centered rotating (Ref. 4)

The Earth-centered rotating (ECR) frame is defined by the instantaneous Earth axes at a specific time. The X axis is on the equator at 0 degrees longitude (the Greenwich Meridian); Z axis in the direction of the Earth north pole; Y axis completes the right-handed triad. The ECR frame is also called the Earth-centered Earth-fixed (ECEF) frame.

3. Orbital

The orbital frame is defined as follows: the Z axis in the direction of the geodetic nadir vector at the orbit position; X axis in the velocity direction and perpendicular to Z; Y axis completes the right-handed triad.

4. Spacecraft

The spacecraft frame can be specified in either an inertial frame or the orbital frame. The axis definitions follow the same convention as the orbital frame: Z downward, X in the direction of motion, Y axis completes the right-handed triad. For PACE, in the mission pointing mode, the spacecraft frame is nominally aligned with the orbital frame except for the yaw steering rotation about the Z axis (ref. 5). The yaw steering is performed to align the SPEXone forward and aft views.

5. Tilt mechanism

The tilt mechanism alignment is specified by the tilt base frame in the spacecraft frame, the tilt rotation axis in the tilt base frame and the forward and aft tilt angles. The tilt platform frame relative to the base frame is determined from the tilt axis and angle. The nominal tilt base axes

are the same as for the spacecraft, and the nominal tilt rotation axis is the Y axis. The nominal tilt angles are +/-20 degrees; the actual values were measured prelaunch.

6. OCI

The OCI reference frame is nominally aligned with the tilt platform frame.

7. J2000 to ECR transformation (Ref. 4)

The J2000 to ECR transformation is calculated as a series of three transformations. The J2000-to-mean-of-date (MOD) transformation, precession, is the slow rotation of the Earth's mean pole around the ecliptic pole of about 50 arcsecond per year. The MOD to true-of-date (TOD) transformation, nutation, is the "wobble" of the Earth's pole around the mean, with a period of 18.6 years and amplitudes of 17.2 degrees in longitude and 9.2 arcseconds in obliquity, the angle between the ecliptic and equatorial planes. The TOD to ECR transformation, the Greenwich hour angle, is the daily rotation of the Earth around the TOD pole, computed from universal time (UT1). The three transformations are applied in that order.

8. ECR to orbital transformation

The ECR to orbital transformation is described in Ref. 6.

9. J2000 to spacecraft transformation

The J2000 to spacecraft transformation is expressed as quaternion (Ref. 7), known in this application as Euler symmetric parameters.

10. Orbital to spacecraft transformation

The orbital to spacecraft transformation is expressed as an Euler angle sequence (Ref. 7), also referred to as roll, pitch and yaw. In the mission pointing mode the roll and pitch are small angles and the yaw is determined by the yaw steering algorithm. The angles are calculated for information only and are not used in the geolocation processing.

11. Spacecraft to tilt base transformation

The spacecraft to tilt base transformation is a small rotation matrix.

12. Tilt base to platform transformation

The tilt base to platform transformation is readily expressed as a quaternion, where the tilt rotation axis is the Euler axis and the tilt angle is the Euler angle.

13. Tilt platform to OCI transformation

The tilt platform to OCI transformation is a small rotation matrix.

B. Inputs to Geolocation

The following data inputs and sources are used for geolocation processing, not including the LUT. The inputs from the spacecraft and instrument telemetry are stored in the Level-1A data products. All data sources are assumed to have accurate time stamps.

- Spacecraft orbit position and velocity. This is provided by either the onboard ephemeris computed by the flight software (FSW) and contained in the spacecraft housekeeping

telemetry (HKT) packets (Ref. 8), or the definitive ephemeris generated by the Mission Operations Center (MOC) Flight Dynamics System (FDS) (Ref 9). The form is cartesian position and velocity vectors in either the J2000 or ECR frame.

- Spacecraft attitude. This is computed by the flight software and contained in the spacecraft HKT packets (Ref. 8). The format is quaternions representing the J2000-to-spacecraft transformation.
- Tilt angles. These are extracted and converted from the spacecraft mechanism control electronics (MCE) telemetry in the HKT packets (Ref. 10).
- OCI scan attributes. The OCI scan start time, spin number and half-angle mirror (HAM) side for each scan are stored as fields in the Level-1A data product.
- OCI telemetry. The OCI MCE (Ref. 11) and Data Acquisition Unit (DAU) Digital Card (DDC) (Ref. 11) telemetry provide the fields that are required for the OCI viewing geometry model. Specific fields and their use are described in section E below.
- OCI mode table. The mode table (Ref. 2) provides the data collect view information that is used to determine the instrument scan angles (e.g. see Figure 1). The mode table fields are extracted from the ancillary packet (Ref. 12). The use of this information is described in Section E.

C. LUT content and format

The OCI geolocation LUT contains instrument parameters, alignment matrices and other non-data information used for geolocation processing. The format is NetCDF, which supports the use of named dimensions and groups to facilitate organization of the file and object-level attributes to describe individual data objects. The detailed file structure in NetCDF Common Data Language (CDL) is in Appendix C. The specific types of information stored in the LUT are:

- OCI clock frequencies
- Coordinate transformations, e.g. spacecraft to tilt base.
- Tilt angles at the fixed positions and the tilt axis.
- RTA and HAM parameters
- Planarity corrections coefficients

The use of these parameters is described in the sections below.

D. Navigation data processing

The navigation fields are needed at the OCI scan times to be used in geolocation. As stated above the OCI scan rate is 5.7 Hz. The navigation fields are provided at lower frequencies. The spacecraft attitude and tilt data at 1 Hz, and the spacecraft ephemeris sample interval is 4 seconds for the onboard ephemeris and 60 seconds for the definitive ephemeris.

The reference times for OCI geolocation correspond to the centers of the science data view (e.g. Earth view for baseline science data collection) for each scan. The calculation of these times is described in the following section.

The tilt measurements during the tilt changes are linearly interpolated to the scan times. The tilt angles at the fixed positions (fore and aft) are set to the LUT values.

The first step in the quaternion processing is to transform the quaternion reference frame from J2000 to ECR. This is performed using the J2000 to ECR transformation matrix described in Section III.A.7 at the quaternion sample time. The transformation matrix is first converted to a quaternion (Ref. 7), which is then used to transform the J2000 quaternion to ECR.

The quaternions are then interpolated using the samples that bracket the scan times, assuming constant rotation rate between quaternions. The rotation quaternion between the bracketing quaternions is computed (Ref. 7):

$$Q_{rot} = Q_i^{-1} Q_{i+1} \quad (1)$$

Where Q_i and Q_{i+1} are the bracketing quaternions, and the product is computed by quaternion multiplication. The spacecraft rotation during 1 second, about 0.061 degree, allows the small angle assumption to be used. The rotation angle and vector are computed using the quaternion vector components:

$$\Theta = | \mathbf{Q_{rot}} | \quad (2)$$

$$\mathbf{E} = \mathbf{Q_{rot}} / | \mathbf{Q_{rot}} | \quad (3)$$

The incremental rotation quaternion is then computed:

$$\Delta t = (t_{scan} - t_i)/(t_{i+1} - t_i) \quad (4)$$

$$\mathbf{Q_{ri}} = E\, \Delta t\, \mathbf{Q_{rot}} \quad (5)$$

Where t_{scan} is the OCI scan time and t_i and t_{i+1} are the sample times of the bracketing quaternions. The scalar component of Q_{ri} is computed by quaternion normalization. The interpolated quaternion at the OCI scan time is then:

$$Q_{scan} = Q_i\, Q_{ri} \quad (6)$$

The interpolation of the ephemeris position and velocity vectors is performed using the method described in Ref. 13, in which the combined position/velocity interpolation is performed between consecutive samples using cubic interpolation.

E. OCI geometry model calculations

The OCI geometry model is used to determine the line-of-sight (LOS) vector for each science pixel in an OCI scan. This involves the following steps:

1. Determination of the OCI line number and time for the center of each science pixel
2. Calculation of the pixel angles from the time offsets and encoder data
3. Determination of the LOS vectors from the angles

These calculations use telemetry from the MCE and the DDC. Each step is described below.

1. Determination of the line number and time for each science pixel

As stated in Section II, each OCI scan consists of a spin of the RTA. The RTA rotation rate is ~5.7 Hz. OCI data collection is performed in multiple zones during a spin. The zone parameters for the current mode are unpacked and stored in the L1A product. The parameters for each zone are the data type, number of lines and aggregation factor. There are data types for Earth collect, dark collect, calibration and diagnostic modes, as well as a No Data type.

Each spin starts at the PPR signal as shown in Figure 1. The PPR corresponds to a specified scan angle that is specified in telemetry as described in the following section. The baseline science-data collection consists of a No Data zone from the PPR to the start of science data collection, an Earth zone, a No Data zone, a Dark zone, and a No data zone, as shown in Table 1.

Each data zone is specified by the number of lines and aggregation factor. A line corresponds to a single, unaggregated data sample from the blue or red FPA. The samples are aggregated according to the aggregation factor to form science pixels; the aggregation factor can be 1, 2, 4 or 8, and is specified separately for each zone. Thus, the actual number of science pixels generated for a zone is the number of lines divided by the aggregation factor. Note that the aggregation factor is referred to in OCI documentation as "i".

Table 1. Mode parameter table for baseline science data collection.

Data Type	(i)	#lines
0 (no data)	1	4784
1 (Earth Col)	8	10120
0 (no data)	1	10840
2 (dark collect)	4	448
0 (no data)	1	6024
0 (no data)	1	0
0 (no data)	1	0
0 (no data)	1	0
0 (no data)	1	0
0 (no data)	1	0

The first line number in a data zone is the sum of the lines from all previous zones. The subsequent lines numbers in that zone will be incremented by the aggregation factor. These line numbers represent the first line number used in each aggregated pixel. To correctly compute the time offset for the center of each science pixel, the line numbers need to be adjusted for both the aggregation factor and the accumulation of each sample output across the 128 rows of the CCD. Thus, the effective line number for pixel n with aggregation i in zone m is:

$$\text{Line}(n) = \sum \text{Lines}(0, n\text{-}1) + n\, i + i/2. - 64 \qquad (7)$$

assuming 0-based pixel numbering.

The time used to calculate the scan angle for each pixel is the offset from the PPR. This is calculated from the line numbers, the master clock frequency and the time-delay integration (TDI) time field in the DDC telemetry. The master clock frequency is specified in the LUT. The TDI time is one less than the number of master clock cycles per line. (This is expected to have the same value for all OCI data.) The time offset for pixel n is calculated as:

$$T_{off}(n) = \text{Line}(n)*(T_{TDI}+1)/F_{MC} \qquad (8)$$

2. Calculation of the pixel scan angles

The LOS angle for each pixel is determined from the scan angle at the PPR time, the time offset from the PPR, the scan rate, and the RTA and HAM angle corrections from their respective encoders.

The PPR scan angle is determined from the PPR offset field in the MCE telemetry and the RTA nadir offset. The latter has values for the primary and redundant MCE boards contained in the LUT. The values are specified in encoder counts, with a revolution being 2^{17} counts. The PPR angle is calculated as:

$$\Theta_{PPR} = 2\pi \, (PPRoff - RTAnad) / 2^{17} \quad (9)$$

For the baseline configuration this calculation gives an angle greater than π, so to generate angles in the range +/-π it is corrected by 2π.

The RTA commanded rotation rate is determined from the Reference Pulse Divider (RPD) in the MCE telemetry. There are two RPD values, one from the DAU and an internal value from the MCE. Another MCE field, the Reference Pulse Select, indicates which one is used. The rate calculated from the DAU RPD uses the master clock frequency:

$$\omega_{RTA} = 2\pi \, F_{MC} / (2^{18} \, (RPD_{DAU}/256 + 1)) \quad (10)$$

while the calculation with the MCE RPD uses the MCE internal clock frequency:

$$\omega_{RTA} = 2\pi \, F_{MCE} / (2^{18} \, (RPD_{MCE}/256 + 1)) \quad (11)$$

Both clock frequencies are stored in the LUT.

The RTA corrections are calculated from the encoder data as follows. The encoder data are sampled at 1 KHz, so during one scan period of 0.1747 s there are 174 or 175 encoder values. The sampling of the encoder data starts at the PPR, so the time offsets are the indices scaled by 0.001 s. The encoder values are the deviations from a uniform rotation rate represented by ω_{RTA}. The sample rate of the baseline science pixels is 23 KHz, so the RTA encoder values will be linearly interpolated to the pixel offset times to determine the corrections.

The corrections using the HAM encoder data are scaled by 0.25 due to the magnification of the primary mirror in the RTA. The scan angle for pixel n is then:

$$\Theta(n) = \Theta_{PPR} + T_{off}(n) \, \omega_{RTA} - \Theta_{corr}(n) \quad (12)$$

3. Determination of the LOS vectors

The geometry of the OCI scan is approximately planar. Deviations from this simple model will results from multiple sources, such as the thickness of the HAM and the HAM side deviations from parallel. These effects were measured during prelaunch geometric testing and incorporated to the LOS vector determination. These deviations, referred to as planarity offsets, are modeled using 4^{th}-order polynomials of the scan angle for the along-scan and along-track offsets. The along-scan correction is applied directly to the scan angle:

$$\Theta_c(n) = \Theta(n) + \Delta P_{AS}(\Theta(n)) \quad (13)$$

The LOS vector calculation is performed as:

$$\mathbf{V}_{LOS}(n) = [\ \sin(\Delta P_{AT}(\Theta(n))),\ \sin(\Theta_c(n)),\ \cos(\Theta_c(n))\ ] \quad (14)$$

Where ΔP_{AS} and ΔP_{AS} are the along-scan and along-track planarity corrections.

F. Ellipsoid geolocation

The ellipsoid geolocation determines the viewed locations on the World Geodetic System 1984 (WGS84) ellipsoid (Ref. 15). It is performed using the method originally developed for the Sea-viewing Wide Field-of-view Sensor (SeaWiFS) (Ref. 6). This method originally assumed a perfectly planar scan geometry. It has since been generalized to three dimensions.

The first step is the determination of the ECR-to-OCI transformation matrix, M. The spacecraft-to-OCI transformation is computed by combining the spacecraft-to-tilt base, tilt rotation and tilt-platform-to-OCI transformations; the first and last are contained in the LUT and the tilt rotation transformation is computed from the tilt axis and angle.

The ECR-to-spacecraft transformation is specified by the interpolated quaternion described in Section III.D. The quaternion is converted to a matrix (Ref. 7) and multiplied by the spacecraft-to-OCI transformation to generate the ECR-to-OCI matrix.

In Ref. 6, if the Y' component is not assumed to be zero, then equation 9 becomes

$$\frac{(M_{1,1}V_{x'} + M_{2,1}V_{y'} + M_{3,1}V_{z'} + P_x)^2}{r_e^2} + \frac{(M_{1,2}V_{x'} + M_{2,2}V_{y'} + M_{32}V_{z'} + P_y)^2}{r_e^2} + \frac{(M_{1,3}V_{x'} + M_{2,3}V_{y'} + M_{33}V_{z'} + P_z)^2}{r_p^2} = 1 \quad (15)$$

where **V** is the sensor-to-surface vector in the OCI frame, **P** is the orbit position vector, and r_e and r_p are the Earth equatorial and polar radii, respectively.

Equation 10 in Ref. 7 becomes

$$AV_{x'}^2 + B\,V_{y'}^2 + C\,V_{z'}^2 + D\,V_{x'}V_{y'} + E\,V_{x'}V_{z'} + F\,V_{y'}V_{z'} + G\,V_{x'} + H\,V_{y'} + I\,V_{z'} + J = 0 \quad (16)$$

where

$$A = M_{1,1}^2 + M_{1,2}^2 + M_{1,3}^2\,(r_e/r_p)^2 \quad (16a)$$
$$B = M_{2,1}^2 + M_{2,2}^2 + M_{2,3}^2\,(r_e/r_p)^2 \quad (16b)$$
$$C = M_{3,1}^2 + M_{3,2}^2 + M_{3,3}^2\,(r_e/r_p)^2 \quad (16c)$$
$$D = 2\,M_{1,1}M_{2,1} + 2\,M_{1,2}M_{2,2} + 2\,M_{1,3}M_{2,3}\,(r_e/r_p)^2 \quad (16d)$$
$$E = 2\,M_{1,1}M_{3,1} + 2\,M_{1,2}M_{3,2} + 2\,M_{1,3}M_{3,3}\,(r_e/r_p)^2 \quad (16e)$$
$$F = 2\,M_{2,1}M_{3,1} + 2\,M_{2,2}M_{3,2} + 2\,M_{2,3}M_{3,3}\,(r_e/r_p)^2 \quad (16f)$$
$$G = 2\,M_{1,1}P_x + 2\,M_{1,2}P_y + 2\,M_{1,3}P_z\,(r_e/r_p)^2 \quad (16g)$$
$$H = 2\,M_{2,1}P_x + 2\,M_{2,2}P_y + 2\,M_{2,3}P_z\,(r_e/r_p)^2 \quad (16h)$$
$$I = 2\,M_{3,1}P_x + 2\,M_{3,2}P_y + 2\,M_{3,3}P_z\,(r_e/r_p)^2 \quad (16i)$$
$$J = P_x^2 + P_y^2 + P_z^2\,(r_e/r_p)^2 - r_e^2 \quad (16j)$$

V can be expressed in terms of its magnitude and a unit cartesian vector:

$$\mathbf{V} = v[x, y, z] \quad (17)$$

where [x, y, z] represents the LOS vector in the sensor frame described in Section III.F.

Substituting into 10, and rearranging, we find that

$$(Ax^2 + By^2 + Cz^2 + Dxy + Exz + Fyz)\,v^2 + (Gx + Hy + Iz)\,v + J = 0 \quad (18)$$

which is solved as a quadratic in v. As described in Ref. 6, the geocentric position vector **G** is then computed as:

$$\mathbf{G} = \mathbf{P} + M^T \mathbf{V} \quad (19)$$

The remaining calculations of the latitude, longitude, solar and sensor zenith and azimuth angles are performed as in Ref. 6.

G. Terrain correction

The terrain correction adjusts the viewed locations and other parameters for the height above the ellipsoid over land and inland water bodies. It uses the method originally developed for MODIS (Ref. 16) and implemented as part of the Ocean Color Science Software (OCSSW) library. The current digital elevation model (DEM) used for the terrain correction is the General Bathymetric Chart of the Oceans 2020 (GEBCO_2020) (Ref. 17).

H. Quality flags

Quality flags are set for geolocation at the scan and pixel level. The flags are bit-mapped, and the specifications are described in the object-level attributes in the Level-1B data product as shown in Appendix B. The scan-level flags indicate the following conditions:

- Tilt change
- Scan time missing (interpolated from adjacent scans)
- Missing MCE encoder data

The pixel-level flags indicate the following conditions:

- Sensor view off Earth
- Terrain correction failed

IV. Calibration Processing

The instrument calibration corrections and their implementation are described in the sections below as follows: calibration equation; calibration LUT content and format; inputs from the Level-1A products; spectral aggregation performed onboard and in ground processing; the radiometric corrections used in the calibration; and the quality flag determination.

A. Calibration equation

OCI science data are calibrated using the following calibration equation (Ref. 18):

$$L_t = K_1 K_2(t) (1 - K_3(T-Tref)) K_4(\theta) K_5(dn) dn \quad (20)$$

Where:

L_t = calibrated radiance
K_1 = absolute gain factor
$K_2(t)$ = relative gain factor as a function of time t
K_3 = temperature correction factor
T = instrument temperatures measured at relevant locations
T_{ref} = reference temperatures (close to expected on-orbit temperatures)
$K_4(\theta)$ = response versus scan angle
θ = scan angle
K_5 = nonlinearity factor
$dn = DN - DN_0$ = dark-corrected DN.
DN = digital number measurement
DN_0 = dark collection DN

Note that the K terms are independent, so the order of multiplication is arbitrary.

B. LUT content and format

The calibration LUT contains all of the parameters needed to compute the corrections listed in the calibration equation, as well as parameters that are stored in the Level-1B product for down-stream processing. The LUT is organized with groups for the individual FPAs (blue, red and SWIR) and a common group. The FPA groups each contain the coefficients for the K_1, K_2, K_3, K_4 and K_5 corrections listed above, along with saturation thresholds and polarization correction coefficients that are stored in the Level-1B product. The SWIR group also contains coefficients for the impulse response correction (Ref. 3). The common group contains the reference times for the K_2 calculation, the reference temperatures for the K_3 calculation, and the band-center wavelengths and solar irradiances for all three FPAs. The LUT format is given in Appendix B.

As indicated by the LUT band dimensions, the coefficients for the blue and red FPAs are stored at full (unaggregated) spectral resolution to support calibration of data collected with any spectral aggregation scheme. This requires that the coefficients themselves need to be aggregated according to the onboard spectral aggregation configuration before being applied to the data. The process for this is described in Section D.3 below.

C. Inputs to Calibration

The instrument radiance measurements are in the form of integers, or DN. As stated in Section II, the red and blue FPA measurements are 16 bits, stored as unsigned short integers in the Level-1A product, and the SWIR FPA measurements are 20 bits stored as long integers. In addition, the following information is used from the Level-1A product:

- Scan attributes, specifically the OCI scan start time, spin number and HAM side for each scan.
- The instrument temperatures that are used in the K_3 correction and their associated times. These are extracted from telemetry packets and stored in the L1A product.
- Spatial zone specifications extracted from the ancillary packet (Ref. 12).
- Spatial and spectral aggregations extracted from the ancillary packet.
- Fill values for the radiance measurements.

D. Spectral aggregation

This section describes the spectral aggregation of OCI hyperspectral (blue and red FPA) data. The initial aggregation is performed by the instrument according to the mode table. Further aggregation is performed during Level-1B calibration processing at SDS. Each stage is described below.

1. Instrument Aggregation

The OCI spectral characteristics are summarized in Section II. As stated, the output from each CCD is collected by 16 "taps", where each tap collects 32 bands. The output bands can be spectrally aggregated by the instrument by factors of 1, 2, 4 or 8, resulting in band-center intervals of 0.625, 1.25, 2.5 and 5 nm, respectively. The aggregation factor ("j") can be set independently for each tap. Data collection for a tap can also be disabled.

The spectral aggregations with j set to 4 and 2 (the values planned for use during baseline Earth data collection) are illustrated in the figures below. Each figure shows the aggregation for a single tap. Figure 2 shows the aggregation with j=4. The output from the 32 CCD columns input to the tap, shown in the first row are aggregated in groups of 4 to generate 8 outputs from that tap, shown in the second row. The aggregation is performed by adding the input samples, which are 14-bit integers, in a 20-bit register and then bit-shifting as needed to generate a 16-bit unsigned integer. (Note that spatial aggregation is also performed, and the combined spectral-spatial aggregation determines the required bit shift.)

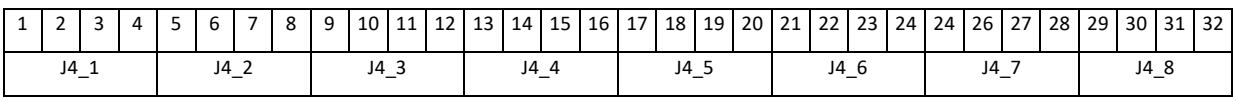

Figure 2 – Spectral aggregation for a tap with j=4, generating 8 outputs at 2.5nm intervals

Figure 3 shows the same aggregation process with j=2. In this case the 32 CCD outputs are aggregated in groups of 2 to generate 16 outputs from the tap.

1	2	3	4	5	6	7	8	9	10	11	12	13	14	15	16	17	18	19	20	21	22	23	24	24	26	27	28	29	30	31	32
J2_1		J2_2		J2_3		J2_4		J2_5		J2_6		J2_7		J2_8		J2_9		J2_10		J2_11		J2_12		J2_13		J2_14		J2_15		J2_16	

Figure 3 – Spectral aggregation for a tap with j=2, generating 16 outputs at 1.25nm intervals.

Following aggregation, the outputs from all of the active taps for each CCD for one science pixel are output in a single CCSDS packet as described in Ref. 2. The j values for each tap are included in the science packets, and also in the ancillary packet once per scan (Ref. 12).

The first stage of processing is Level-0-to-1A. During this processing, the science data samples are extracted from the packets and written to data arrays in the Level-1A data product; the samples are not altered in any way at this step.

2. Level-1B Processing Aggregation

The Level-1B processing includes a second aggregation step; the purpose is to improve the signal-to-noise ratio (SNR) of the science data, while maintaining the spectral sampling from the instrument. This is performed by combining the input samples to generate the equivalent of 8x aggregation, while maintaining the spectral sampling from the instrument.

This process is illustrated in Figure 4 for data from two adjacent taps with 4x aggregation. The samples in the second row labeled A and B are those generated by the instrument from the two taps. The remaining rows with samples labeled O are the aggregated samples generated during L1B processing. The figure shows how each input sample is used in two outputs in order to maintain the 2.5 nm. This method preserves the band-center spacing from the input samples while increasing the SNR. The figure shows how one of the output samples is generated using one sample from each tap in order to maintain the 2.5 nm band-center interval across the tap boundary. This processing is continued across all taps that use 4x aggregation.

Tap A									**Tap B**							
A1	A2	A3	A4	A5	A6	A7	A8		B1	B2	B3	B4	B5	B6	B7	B8
O1		O3		O5		O7			O9		O11		O13		O15	
	O2		O4		O6		O8			O10		O12		O14		

Figure 4 – Generation of 8x aggregated bands using 4x aggregated input samples from adjacent taps during L1B processing.

The processing is similar for taps with 2x aggregation. This is illustrated in Figure 5, which shows half of the 16 inputs from each of two adjacent taps and the corresponding L1B outputs. In this case, each input sample is used in four output samples to maintain the 1.25 nm interval; in this case, three of the output samples use inputs from both taps.

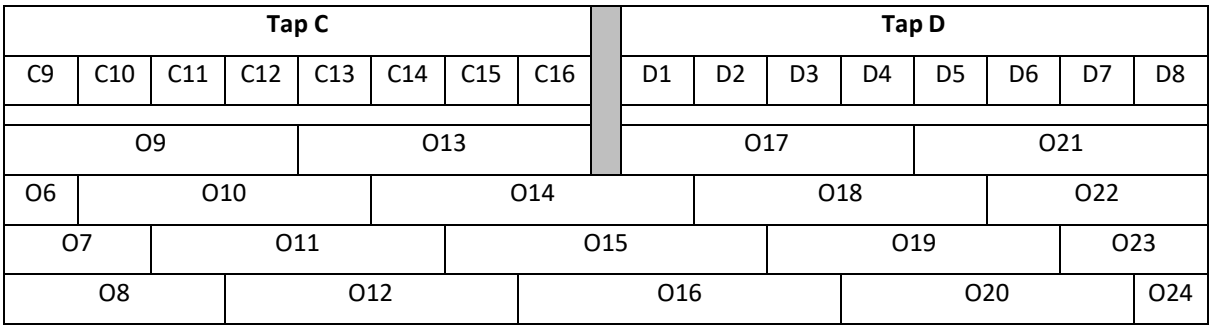

Figure 5 – Generation of 8x aggregated bands using 2x aggregated input samples from adjacent taps during L1B processing.

The L1B aggregation is more complicated at the boundary between taps with different aggregation factors. Output samples with the smaller band center interval can only be generated when all of the input sample are from the tap with the smaller aggregation factor. This is illustrated in Figure 6 for adjacent taps with 4x and 2x aggregation. I n this case, the 2.5nm band-center interval continues up to the first output sample generated from the second tap; from that point through the remaining inputs from that tap, the output band-center interval is 1.25nm. Also, each input band will be weighted in proportion to its instrument aggregation factor; thus, to generate output band O8, input E8 will be weighted twice as much as F1 and F2.

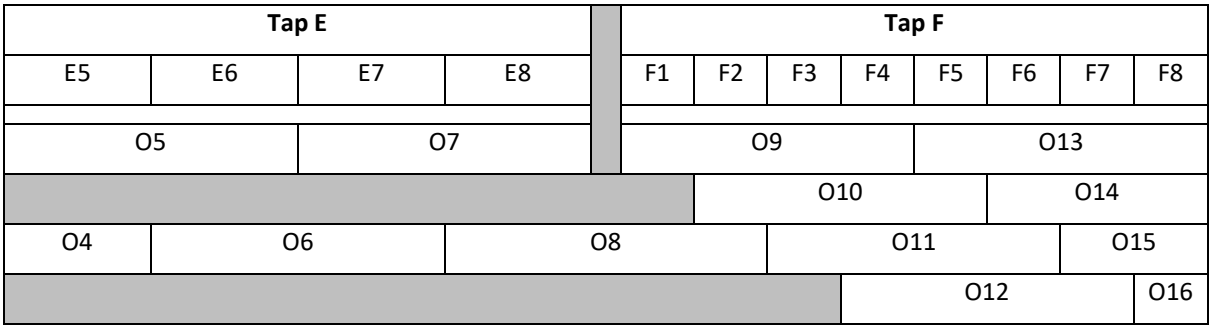

Figure 6 – Generation of 8x aggregated bands across the transition from 4x to 2x aggregation.

Note that the number of output bands from this process will be slightly fewer that the number of input. The reason is that the first and last samples from a CCD can only be used in one output. Transitions between adjacent taps with different aggregation factors will also result in fewer output bands. The number of output bands is calculated for each CCD from the aggregation factors (and enable/disable states) for all 16 taps, along with the band-center wavelengths for each band.

It should also be noted that the band center wavelengths for the L1B aggregated bands will be different from those of the instrument bands, although the band-center intervals will be maintained. This can be understood by examination of Figures 4 through 6. For example, in Figure 6, the center wavelength for output band O5 will be the average of those for input bands E5 and E6, O8 will have the weighted average of E8, F1 and F2, and O10 will have the average of F2 through F5.

3. Implementation of Aggregation

The implementation of spectral aggregation within the calibration processing is twofold:

- Aggregate the correction coefficients in the LUT according to the instrument aggregation configuration. This is required in order to correctly calculate the corrections listed in Section A for the aggregated data.
- Re-aggregate the spectral band data to achieve 8x aggregation across the spectral range for each FPA.

Both of these are accomplished by generating matrices that are used to perform the aggregation with appropriate weighing. The matrices are generated separately for the two FPAs, as each FPA can have a different spectral aggregation scheme. As stated above, the LUT coefficients are all stored for 8x1 (i x j) aggregation, with a band dimension of 512. The coefficient aggregation matrix therefore has dimensions N x 512, where N is the number of bands generated by the instrument for the FPA. In the baseline science mode, the spectral aggregation factor is 4 for all the blue FPA taps, while for the red FPA there are two groups of taps with 2x aggregation. This results in 120 blue bands and 168 red bands. The matrix is band-diagonal, and the non-zero values are the weighting factors for the coefficient aggregation.

Adjustments are required for the K1 and K5 coefficients for the blue and red FPAs if the combined aggregation is less than 4. In these cases, the effective number of bits in the dn are reduced to 14 (1x1) or 15 (1x2 or 2x1). Because these coefficients are applied to the dn, they are adjusted to correctly calculate the absolute gain and linearity corrections.

The matrix for the re-aggregation follows the approach illustrated in Figures 4 through 6, in which radiances collected at 4x or 2x spectral aggregation are combined to produce 8x values. As stated in Section 2, this reduces the number of output bands. In the baseline science mode, the result is 119 blue bands and 163 red bands. If this number is M, the re-aggregation matrix dimensions are N x M.

E. Radiometric corrections

The implementation of the radiometric corrections is described in the following sections: dark count, K1 through K5, SWIR band hysteresis, stray light and conversion to reflectance. Additional details regarding the radiometric corrections can be found in Ref. 18.

1. Dark count

The instrument measurements are biased to ensure that all of the values of the unsigned integers are positive at zero radiance. The dark count is measured every scan at the dark view shown in Figure 1. In the baseline science mode there are 57 pixels per scan in the dark view. The data from this view are averaged scan-by-scan to compute the DN_0 used to convert DN to dn as in Equation 20. The averaging is currently a simple arithmetic mean, although a robust mean is under consideration to account for noise spikes in the data.

Unlike the science data views, the dark view data are not bit-shifted after being aggregated onboard; therefore the dark data need to be adjusted to compute the equivalent bit-shifted value if the science data are collected with a combined aggregation greater than 4, as is the case for the baseline science. For these cases, the dark view is divided by (i x j)/4.

2. Absolute gains (K1)

The K1 values are stored in the LUT as one value per band and HAM side. The units are radiance units (watts per m^2 per micron per steradian). As described in Section D.3, following aggregation to the instrument configuration the values are adjusted if needed.

3. Temporal response (K2)

The K2 values are stored in the LUT as a series of time-tagged values per band and mirror side. These values are updated regularly to extend the time range based on analysis of the solar and lunar calibration data (Ref. 18). The form of the time tags is floating point days since January 1, 2000. For each granule, the granule mid-time is used to identify the bounding set of K2 values and interpolate them to the granule time.

4. Temperature (K3)

The temperature correction shown in Equation 20 is implemented as a quadratic function of ($T - T_{ref}$). The K3 coefficients are stored in the LUT as a set of values per band and temperature. Currently the correction is linear and the second-order coefficients in the LUT are set to zero. During prelaunch instrument characterization testing, a set of temperatures was identified for the temperature correction for each FPA and the coefficients were determined. These are listed in Table 2. The blue and red FPA corrections use the first eight temperatures in the list, and the remaining temperatures are used for the SWIR band corrections. As stated in Section B, the reference temperatures for each temperature in the table are also stored in the LUT.

5. RVS (K4)

The RVS correction is implemented as a 4^{th}-order polynomial of the scan angle in radians. The inputs are the scan angles computed using Equation 12 in Section III. The K4 coefficients are stored in the LUT per band and HAM side. For the SWIR bands there are also separate sets of coefficients for the two MCE boards. The RVS was measured and the coefficients determined during prelaunch characterization testing. The constant term is assumed to be unity to normalize the corrections at the nadir pixel. A set of constant values for the solar calibrator assembly (SCA) view is also stored for each band and used to correct the solar calibration data.

6. Linearity (K5)

The linearity correction is implemented as a 4^{th}-order polynomial of dn. The K5 coefficients are stored in the LUT per band. Unlike the K4, the constant term is not unity and is included in the LUT.

7. SWIR band hysteresis

As stated in Section II, the SWIR bands have an extended response to bright sources (Ref. 3). A correction for this response, also called hysteresis, was developed (Ref. 19) and implemented in the calibration software. As described in the reference, the hysteresis is modeled as a sum of decaying exponential functions with different amplitudes and time constants. The correction is computed recursively for a pixel using the radiances from all up-scan pixels. The current implementation includes up to four exponential functions. The amplitudes and time constants are stored in the calibration LUT.

Table 2. OCI Temperatures Used for Temperature Correction

Description	**Thermal Mnemonic**
UVVIS Lens Housing (CCD side)	oci.ptlm.Therm.Temp.UvvisLensHousingCcd
UVVIS Lens Housing (grating side)	oci.ptlm.Therm.Temp.UvvisLensHousingGrating
VISNIR Lens Housing (CCD side)	oci.ptlm.Therm.Temp.VisnirLensHousingCcd
VISNIR Lens Housing (grating side)	oci.ptlm.Therm.Temp.VisnirLensHousingGrating
VISNIR FEE Temp Sensor at CCD Right Side	oci.ptlm.Therm.Temp.VisnirCcdRight
VISNIR FEE Temp Sensor at CCD Left Side	oci.ptlm.Therm.Temp.VisnirCcdLeft
UVVIS FEE Temp Sensor at CCD Right Side	oci.ptlm.Therm.Temp.UvvisCcdRight
UVVIS FEE Temp Sensor at CCD Left Side	oci.ptlm.Therm.Temp.UvvisCcdLeft
SDS_DET_TEMP1 (SdsDetectorTemp1)	oci.ptlm.Therm.Temp.SdsAssembly1
SDS_DET_TEMP2 (SdsDetectorTemp2)	oci.ptlm.Therm.Temp.SdsAssembly2
SDS_DET_TEMP3 (SdsDetectorTemp3)	oci.ptlm.Therm.Temp.SdsAssembly3
SDS_DET_TEMP4 (SdsDetectorTemp4)	oci.ptlm.Therm.Temp.SdsAssembly4
SDS_DET_TEMP5 (SdsDetectorTemp5)	oci.ptlm.Therm.Temp.SdsAssembly5
SDS_DET_TEMP6 (SdsDetectorTemp6)	oci.ptlm.Therm.Temp.SdsAssembly6
SDS_DET_TEMP7 (SdsDetectorTemp7)	oci.ptlm.Therm.Temp.SdsAssembly7
SDS_DET_TEMP8 (SdsDetectorTemp8)	oci.ptlm.Therm.Temp.SdsAssembly8
SDS_DET_TEMP9 (SdsDetectorTemp9)	oci.ptlm.Therm.Temp.SdsAssembly9
SDS_DET_TEMP10 (SdsDetectorTemp10)	oci.ptlm.Therm.Temp.SdsAssembly10
SDS_DET_TEMP11 (SdsDetectorTemp11)	oci.ptlm.Therm.Temp.SdsAssembly11
SDS_DET_TEMP12 (SdsDetectorTemp12)	oci.ptlm.Therm.Temp.SdsAssembly12
SDS_DET_TEMP13 (SdsDetectorTemp13)	oci.ptlm.Therm.Temp.SdsAssembly13
SDS_DET_TEMP14 (SdsDetectorTemp14)	oci.ptlm.Therm.Temp.SdsAssembly14
SDS_DET_TEMP15 (SdsDetectorTemp15)	oci.ptlm.Therm.Temp.SdsAssembly15
SDS_DET_TEMP16 (SdsDetectorTemp16)	oci.ptlm.Therm.Temp.SdsAssembly16
AOB_TEMP1_S (AobTemp1)	oci.ptlm.Therm.Temp.AobNearSds1
AOB_TEMP2_S (AobTemp2)	oci.ptlm.Therm.Temp.AobNearSds4
AOB_TEMP3_S (AobTemp3)	oci.ptlm.Therm.Temp.AobNearSds6and7
AOB_TEMP4_S (AobTemp4)	oci.ptlm.Therm.Temp.AobNearSds6and10
AOB_TEMP7_S (AobTemp7)	oci.ptlm.Therm.Temp.AobNearSds9
AOB_TEMP8_S (AobTemp8)	oci.ptlm.Therm.Temp.AobNearSds12
MOSB near MLA	oci.ptlm.Therm.Temp.MosbNearMla

8. Stray light and crosstalk

The correction for stray light and crosstalk is TBD.

9. Reflectance conversion

The calibrated values for Earth-viewing data are stored in the Level-1B product as reflectance. This is computed from the calibrated radiance as:

$$\rho_t = L_t * \pi * d^2_{ES} / (F_0 \cos(\theta)) \quad (21)$$

where:

ρ_t = top-of-atmosphere reflectance for earth view pixel
L_t = TOA radiance from equation 20
d_{ES} = earth-sun distance (normalized to 1 astronomical unit)
F_0 = extraterrestrial solar irradiance (solar constant from TSIS (Ref. 20) or other source)
θ = solar zenith incidence angle at pixel location, computed as in Section III.F.

F. Quality flags

Quality flags are set for the calibrated data at the pixel level. The flags are bit-mapped, and the specifications are described in the object-level attributes in the Level-1B data product as shown in Appendix B.

Currently the only condition set in the flags is saturation of the measurements. Saturation occurs at DN values below the maximum for the measurement data type (e.g., 65535 for the 16-bit hyperspectral measurements) and was determined during prelaunch measurements as the value at which the radiance-to-DN relationship becomes substantially nonlinear. The saturation thresholds are based on dn for the blue and red bands and DN for the SWIR bands and are stored in the calibration LUT.

V. Level-1B Product Format

The OCI Level-1B data product is formatted using NetCDF4. It uses named dimensions to give context to the data object dimensions and logically relate objects with similar characteristics. It also follows standard conventions for object-level attributes. The product is organized as follows.

Global attributes are used to store product-level metadata, following conventions (Climate / Forecast and Attribute Convention for Data Discovery) and Ocean Biology Processing Group (OBPG) standard practice.

The **sensor_band_parameters** group contains descriptive information about the spectral bands, including the band-center wavelengths and extraterrestrial solar irradiance values (F_0 in Equation 21) for all three FPAs, the SWIR bandpasses, and the polarization coefficients used for the Level-2 processing.

The **scan_line_attributes** group contains the scan time (mid-time of the science data view), HAM side and scan-level quality flag.

The **geolocation_data** group contains the output of the geolocation processing for each pixel, specifically the latitude, longitude, terrain height, sensor zenith and azimuth, solar zenith and azimuth, and quality flag. Note that the pixels-per-scan dimension for these data objects is for the blue and red bands; if the spatial aggregation factor is less than 8, the dimension will be a multiple of that for the SWIR bands, and the geolocation data need to be resampled along-scan for use with the SWIR bands.

The **navigation_data** group contains the input data used for the geolocation processing, specifically the attitude and ephemeris data interpolated to the scan times, tilt angles, reference Sun vector, and scan angles computed as described in Section III.D.2. The spacecraft attitude angles (roll, pitch and yaw) are included for information only.

The **observation_data** group contains the calibrated measurement data for all three FPAs and the associated pixel-level quality flags. The calibrated measurements can be stored as either reflectance (ρ_t) or radiance (L_t); the former is used for Earth-viewing data and the latter for solar and lunar calibration measurements.

A sample product format in NetCDF CDL is shown in Appendix A.

References

1. Meister G., et al. 2024. "The Ocean Color Instrument (OCI) on the Plankton, Aerosol, Cloud, ocean Ecosystem (PACE) Mission: System Design and Prelaunch Radiometric Performance." IEEE Transactions on Geoscience and Remote Sensing 1-1 [10.1109/tgrs.2024.3383812]
2. Haddad, O., "DAU Digital Card (DDC) FPGA Specification", OCI-ELEC-SPEC-0009, Rev. C, March 2022.
3. Gliese, U., et al., "Pulse Response of the Short-Wave Infrared Detection System of the Ocean Color Instrument for the NASA PACE Mission," SPIE SPIE Sensors + Imaging 2023, Amsterdam, NL.
4. Seidelmann, P. K., ed., *Explanatory Supplement to the Astronomical Almanac,* University Science Books, 1992.
5. Patt, F., "PACE Yaw Steering to Support SPEXone Science Data Collection," PACE-SYS-ANYS-0065, November 2018.
6. Patt, F. and W. Gregg, "Exact closed-form geolocation algorithm for Earth survey sensors," *Int. J. Remote Sensing*, Vol. 15, No. 18, 1994.
7. Wertz, J. R., ed., *Spacecraft Attitude Determination and Control*, D. Reidel, 1978.
8. Galante, J., "ACS FSW Build ICDs," PACE-GNC-ICD-0108, July 2023.
9. Robinson, J., PACE Mission Operations Center (MOC) to Science Data Segment (SDS) Interface Requirements Document (IRD) / Interface Control Document (ICD), PACE-OPS-ICD-0009, Rev. D, September 2022.
10. Lee, K., "PACE Tilt and Solar Array Drive Electronic (TSADE) 1553 Data Interface Control Document," PACE-MECSM-ICD-0062, Rev. C, June 2022.
11. Capon, T., "OCI MCE FPGA Specification," OCI-MECH-SPEC-0050, Rev. E, February 2022.
12. Chemerys, L., "OCI Ancillary Packet Definition," OCI-SYS-DESC-0063, Rev. E, April 2023.
13. Patt, F., "Navigation Algorithms for the SeaWiFS Mission," *SeaWiFS Postlaunch Technical Report Series*, NASA/TM-2002-206892, Vol. 16, S. Hooker and E. Firestone, eds., February 2002.
14. Capon, T. and L. Chemerys, private communication, 2020.
15. "World Geodetic System 1984 (WGS 84)," Office of Geomatics, National Geospatial-Intelligence Agency. https://earth-info.nga.mil/?dir=wgs84&action=wgs84
16. Nishihama, M., et al., "MODIS Level 1A Earth Location: Algorithm Theoretical Basis Document", V3.0, August 1997. https://modis.gsfc.nasa.gov/data/atbd/atbd_mod28.pdf
17. Wetherall, P., "The GEBCO_2020 Grid - a continuous terrain model of the global oceans and land," British Oceanographic Data Centre, National Oceanography Centre, NERC, April 2020.
18. Meister, G., "OCI On-Orbit Calibration Plan," OCI-SCI-PLAN-0124, Rev. B, November 2021.
19. Patt, F., "Development of a Software Correction for the PACE OCI SWIR Band Hysteresis," *PACE Technical Report Series,* NASA/TM-2018-219027, Vol. 13, I. Cetinic, C. R. McClain and P. J. Werdell, eds., TBD.
20. Coddington, O. M., "Version 2 of the TSIS-1 Hybrid Solar Reference Spectrum and Extension to the Full Spectrum," *AGU Earth and Space Science*, Vol. 10, Issue 3, January 2023.

Appendix A – OCI Level-1B Product CDL

The OCI Level-1B data product format is shown below for a sample data product.

```
netcdf PACE_OCI.20240521T003442.L1B {
dimensions:
        number_of_scans = 1710 ;
        ccd_pixels = 1272 ;
        SWIR_pixels = 1272 ;
        blue_bands = 119 ;
        red_bands = 163 ;
        SWIR_bands = 9 ;
        vector_elements = 3 ;
        quaternion_elements = 4 ;
        polarization_coefficients = 3 ;
        HAM_sides = 2 ;
// global attributes:
                :title = "PACE OCI Level-1B Data" ;
                :instrument = "OCI" ;
                :product_name = "PACE_OCI.20240521T003442.L1B.nc" ;
                :processing_version = "V1.0" ;
                :processing_level = "L1B" ;
                :cdm_data_type = "swath" ;
                :geospatial_lat_units = "degrees_north" ;
                :geospatial_lon_units = "degrees_east" ;
                :CDL_version_date = "2024-03-14" ;
                :rta_nadir = 162, 17 ;
                :creator_name = "NASA/GSFC/OBPG" ;
                :creator_email = "data@oceancolor.gsfc.nasa.gov" ;
                :creator_url = "https://oceancolor.gsfc.nasa.gov" ;
                :institution = "NASA Goddard Space Flight Center, Ocean Biology Processing Group" ;
                :license = "https://www.earthdata.nasa.gov/engage/open-data-services-and-software/data-and-
information-policy" ;
                :naming_authority = "gov.nasa.gsfc.oceancolor" ;
                :project = "Ocean Biology Processing Group" ;
                :publisher_name = "NASA/GSFC/OB.DAAC" ;
                :publisher_email = "data@oceancolor.gsfc.nasa.gov" ;
                :publisher_url = "https://oceancolor.gsfc.nasa.gov" ;
                :Conventions = "CF-1.8, ACDD-1.3" ;
                :standard_name_vocabulary = "CF Standard Name Table v79" ;
                :keywords_vocabulary = "NASA Global Change Master Directory (GCMD) Science Keywords" ;
                :date_created = "2024-05-21T02:26:43.000Z" ;
                :earth_sun_distance_correction = 1.02437896916602 ;
                :geospatial_lat_min = 0.9625648f ;
                :geospatial_lat_max = 23.97286f ;
                :geospatial_lon_min = -180.f ;
                :geospatial_lon_max = 180.f ;
                :geospatial_bounds_crs = "EPSG:4326" ;
                :history = "2024-05-21T02:11:41Z: l1agen_oci OCI_temp.L0 5 -t 20240521T003442 -k”
                :time_coverage_start = "2024-05-21T00:34:42.067" ;
                :time_coverage_end = "2024-05-21T00:39:41.949" ;
```

```
group: sensor_band_parameters {
  variables:
        float blue_wavelength(blue_bands) ;
                blue_wavelength:_FillValue = -32767.f ;
                blue_wavelength:long_name = "Band center wavelengths for bands from blue CCD" ;
                blue_wavelength:valid_min = 305.f ;
                blue_wavelength:valid_max = 610.f ;
                blue_wavelength:units = "nm" ;
        float red_wavelength(red_bands) ;
                red_wavelength:_FillValue = -32767.f ;
                red_wavelength:long_name = "Band center wavelengths for bands from red CCD" ;
                red_wavelength:valid_min = 595.f ;
                red_wavelength:valid_max = 900.f ;
                red_wavelength:units = "nm" ;
        float SWIR_wavelength(SWIR_bands) ;
                SWIR_wavelength:_FillValue = -32767.f ;
                SWIR_wavelength:long_name = "Band center wavelengths for SWIR bands" ;
                SWIR_wavelength:valid_min = 900.f ;
                SWIR_wavelength:valid_max = 2260.f ;
                SWIR_wavelength:units = "nm" ;
        float SWIR_bandpass(SWIR_bands) ;
                SWIR_bandpass:_FillValue = -32767.f ;
                SWIR_bandpass:long_name = "Bandpasses for SWIR bands" ;
                SWIR_bandpass:valid_min = 0.f ;
                SWIR_bandpass:valid_max = 100.f ;
                SWIR_bandpass:units = "nm" ;
        float blue_solar_irradiance(blue_bands) ;
                blue_solar_irradiance:_FillValue = -32767.f ;
                blue_solar_irradiance:long_name = "Mean extraterrestrial solar irradiance at 1 astronomical unit
for the wavelengths of the blue CCD" ;
                blue_solar_irradiance:valid_min = 0.f ;
                blue_solar_irradiance:valid_max = 2500.f ;
                blue_solar_irradiance:units = "W m^-2 um^-1" ;
        float red_solar_irradiance(red_bands) ;
                red_solar_irradiance:_FillValue = -32767.f ;
                red_solar_irradiance:long_name = "Mean extraterrestrial solar irradiance at 1 astronomical unit
for the wavelengths of the red CCD" ;
                red_solar_irradiance:valid_min = 0.f ;
                red_solar_irradiance:valid_max = 2500.f ;
                red_solar_irradiance:units = "W m^-2 um^-1" ;
        float SWIR_solar_irradiance(SWIR_bands) ;
                SWIR_solar_irradiance:_FillValue = -32767.f ;
                SWIR_solar_irradiance:long_name = "Mean extraterrestrial solar irradiance at 1 astronomical
unit for the SWIR wavelengths" ;
                SWIR_solar_irradiance:valid_min = 0.f ;
                SWIR_solar_irradiance:valid_max = 2500.f ;
                SWIR_solar_irradiance:units = "W m^-2 um^-1" ;
        float blue_m12_coef(blue_bands, HAM_sides, polarization_coefficients) ;
                blue_m12_coef:long_name = "Blue band M12/M11 polynomial coefficients" ;
                blue_m12_coef:units = "dimensionless" ;
        float blue_m13_coef(blue_bands, HAM_sides, polarization_coefficients) ;
                blue_m13_coef:long_name = "Blue band M13/M11 polynomial coefficients" ;
                blue_m13_coef:units = "dimensionless" ;
```

```
        float red_m12_coef(red_bands, HAM_sides, polarization_coefficients) ;
                red_m12_coef:long_name = "Red band m12/M11 polynomial coefficients" ;
                red_m12_coef:units = "dimensionless" ;
        float red_m13_coef(red_bands, HAM_sides, polarization_coefficients) ;
                red_m13_coef:long_name = "Red band M13/M11 polynomial coefficients" ;
                red_m13_coef:units = "dimensionless" ;
        float SWIR_m12_coef(SWIR_bands, HAM_sides, polarization_coefficients) ;
                SWIR_m12_coef:long_name = "SWIR band M12/M11 polynomial coefficients" ;
                SWIR_m12_coef:units = "dimensionless" ;
        float SWIR_m13_coef(SWIR_bands, HAM_sides, polarization_coefficients) ;
                SWIR_m13_coef:long_name = "SWIR band M13/M11 polynomial coefficients" ;
                SWIR_m13_coef:units = "dimensionless" ;
 } // group sensor_band_parameters

group: scan_line_attributes {
 variables:
        double time(number_of_scans) ;
                time:_FillValue = -32767. ;
                time:long_name = "time" ;
                time:valid_min = 0. ;
                time:valid_max = 172802. ;
                time:description = "Earth view mid time in seconds of day" ;
                time:units = "seconds since 2024-05-21 00:00:00" ;
        ubyte HAM_side(number_of_scans) ;
                HAM_side:_FillValue = 255UB ;
                HAM_side:long_name = "Half-angle mirror side" ;
                HAM_side:valid_min = 0UB ;
                HAM_side:valid_max = 1UB ;
        ubyte scan_quality_flags(number_of_scans) ;
                scan_quality_flags:_FillValue = 255UB ;
                scan_quality_flags:long_name = "Scan quality flags " ;
                scan_quality_flags:flag_masks = 1UB, 2UB, 4UB ;
                scan_quality_flags:flag_meanings = "tilt_change missing_time missing_encoder" ;
                scan_quality_flags:units = "none" ;
 } // group scan_line_attributes

group: geolocation_data {
 variables:
        float latitude(number_of_scans, ccd_pixels) ;
                latitude:_FillValue = -32767.f ;
                latitude:long_name = "Latitudes of pixel locations" ;
                latitude:valid_min = -90.f ;
                latitude:valid_max = 90.f ;
                latitude:units = "degrees_north" ;
        float longitude(number_of_scans, ccd_pixels) ;
                longitude:_FillValue = -32767.f ;
                longitude:long_name = "Longitudes of pixel locations" ;
                longitude:valid_min = -180.f ;
                longitude:valid_max = 180.f ;
                longitude:units = "degrees_east" ;
```

```
        short height(number_of_scans, ccd_pixels) ;
                height:_FillValue = -32767s ;
                height:long_name = "Terrain height at pixel locations" ;
                height:valid_min = -1000s ;
                height:valid_max = 10000s ;
                height:units = "meters" ;
        short sensor_azimuth(number_of_scans, ccd_pixels) ;
                sensor_azimuth:_FillValue = -32767s ;
                sensor_azimuth:long_name = "Sensor azimuth angle at pixel locations" ;
                sensor_azimuth:valid_min = -18000s ;
                sensor_azimuth:valid_max = 18000s ;
                sensor_azimuth:scale_factor = 0.01 ;
                sensor_azimuth:add_offset = 0. ;
                sensor_azimuth:units = "degrees" ;
        short sensor_zenith(number_of_scans, ccd_pixels) ;
                sensor_zenith:_FillValue = -32767s ;
                sensor_zenith:long_name = "Sensor zenith angle at pixel locations" ;
                sensor_zenith:valid_min = 0s ;
                sensor_zenith:valid_max = 18000s ;
                sensor_zenith:scale_factor = 0.01 ;
                sensor_zenith:add_offset = 0. ;
                sensor_zenith:units = "degrees" ;
        short solar_azimuth(number_of_scans, ccd_pixels) ;
                solar_azimuth:_FillValue = -32767s ;
                solar_azimuth:long_name = "Solar azimuth angle at pixel locations" ;
                solar_azimuth:valid_min = -18000s ;
                solar_azimuth:valid_max = 18000s ;
                solar_azimuth:scale_factor = 0.01 ;
                solar_azimuth:add_offset = 0. ;
                solar_azimuth:units = "degrees" ;
        short solar_zenith(number_of_scans, ccd_pixels) ;
                solar_zenith:_FillValue = -32767s ;
                solar_zenith:long_name = "Solar zenith angle at pixel locations" ;
                solar_zenith:valid_min = 0s ;
                solar_zenith:valid_max = 18000s ;
                solar_zenith:scale_factor = 0.01 ;
                solar_zenith:add_offset = 0. ;
                solar_zenith:units = "degrees" ;
        ubyte quality_flag(number_of_scans, ccd_pixels) ;
                quality_flag:_FillValue = 255UB ;
                quality_flag:long_name = "Geolocation pixel quality flags" ;
                quality_flag:flag_masks = 1UB, 2UB, 4UB ;
                quality_flag:flag_meanings = "Off_Earth Input_invalid Terrain_bad" ;
 } // group geolocation_data

group: navigation_data {
 variables:
        float att_quat(number_of_scans, quaternion_elements) ;
                att_quat:_FillValue = -32767.f ;
                att_quat:long_name = "Attitude quaternions at EV mid-times" ;
                att_quat:valid_min = -1.f ;
                att_quat:valid_max = 1.f ;
```

```
        float att_ang(number_of_scans, vector_elements) ;
                att_ang:_FillValue = -32767.f ;
                att_ang:long_name = "Attitude angles (roll, pitch, yaw) at EV mid-times" ;
                att_ang:valid_min = -180.f ;
                att_ang:valid_max = 180.f ;
                att_ang:units = "degrees" ;
        float orb_pos(number_of_scans, vector_elements) ;
                orb_pos:_FillValue = -9999999.f ;
                orb_pos:long_name = "Orbit position vectors at EV mid-times (ECR)" ;
                orb_pos:valid_min = -7100000.f ;
                orb_pos:valid_max = 7100000.f ;
                orb_pos:units = "meters" ;
        float orb_vel(number_of_scans, vector_elements) ;
                orb_vel:_FillValue = -32767.f ;
                orb_vel:long_name = "Orbit velocity vectors at EV mid-times (ECR)" ;
                orb_vel:valid_min = -7600.f ;
                orb_vel:valid_max = 7600.f ;
                orb_vel:units = "meters/second" ;
        float sun_ref(number_of_scans, vector_elements) ;
                sun_ref:_FillValue = -32767.f ;
                sun_ref:long_name = "Solar unit vectors in J2000 frame" ;
                sun_ref:valid_min = -1.f ;
                sun_ref:valid_max = 1.f ;
        float tilt_angle(number_of_scans) ;
                tilt_angle:_FillValue = -32767.f ;
                tilt_angle:long_name = "Tilt angles at EV mid-times" ;
                tilt_angle:valid_min = -21.f ;
                tilt_angle:valid_max = 21.f ;
        float CCD_scan_angles(number_of_scans, ccd_pixels) ;
                CCD_scan_angles:_FillValue = -32767.f ;
                CCD_scan_angles:long_name = "Scan angles for blue and red band science pixels" ;
                CCD_scan_angles:valid_min = -110.f ;
                CCD_scan_angles:valid_max = 250.f ;
                CCD_scan_angles:units = "degrees" ;
        float SWIR_scan_angles(number_of_scans, SWIR_pixels) ;
                SWIR_scan_angles:_FillValue = -32767.f ;
                SWIR_scan_angles:long_name = "Scan angles for SWIR band science pixels" ;
                SWIR_scan_angles:valid_min = -110.f ;
                SWIR_scan_angles:valid_max = 250.f ;
                SWIR_scan_angles:units = "degrees" ;
 } // group navigation_data

group: observation_data {
 variables:
        float rhot_blue(blue_bands, number_of_scans, ccd_pixels) ;
                rhot_blue:_FillValue = -32767.f ;
                rhot_blue:long_name = "Top of Atmosphere Blue Band Reflectance" ;
                rhot_blue:valid_min = 0.f ;
                rhot_blue:valid_max = 1.3f ;
                rhot_blue:units = "dimensionless" ;
                rhot_blue:description = "rhot = Lt * Pi * earth_sun_distance_correction/(solar_irradiance *
cos(solar_zenith))" ;
```

```
        ubyte qual_blue(blue_bands, number_of_scans, ccd_pixels) ;
                qual_blue:_FillValue = 255UB ;
                qual_blue:long_name = "Blue Band Quality Flag" ;
                qual_blue:flag_masks = 1UB ;
                qual_blue:flag_meanings = "saturation" ;
        float rhot_red(red_bands, number_of_scans, ccd_pixels) ;
                rhot_red:_FillValue = -32767.f ;
                rhot_red:long_name = "Top of Atmosphere Red Band Reflectance" ;
                rhot_red:valid_min = 0.f ;
                rhot_red:valid_max = 1.3f ;
                rhot_red:units = "dimensionless" ;
                rhot_red:description = "rhot = Lt * Pi * earth_sun_distance_correction/(solar_irradiance *
cos(solar_zenith))" ;
        ubyte qual_red(red_bands, number_of_scans, ccd_pixels) ;
                qual_red:_FillValue = 255UB ;
                qual_red:long_name = "Red Band Quality Flag" ;
                qual_red:flag_masks = 1UB ;
                qual_red:flag_meanings = "saturation" ;
        float rhot_SWIR(SWIR_bands, number_of_scans, SWIR_pixels) ;
                rhot_SWIR:_FillValue = -32767.f ;
                rhot_SWIR:long_name = "Top of Atmosphere SWIR Band Reflectance" ;
                rhot_SWIR:valid_min = 0.f ;
                rhot_SWIR:valid_max = 1.3f ;
                rhot_SWIR:units = "dimensionless" ;
                rhot_SWIR:description = "rhot = Lt * Pi * earth_sun_distance_correction/(solar_irradiance *
cos(solar_zenith))" ;
        ubyte qual_SWIR(SWIR_bands, number_of_scans, SWIR_pixels) ;
                qual_SWIR:_FillValue = 255UB ;
                qual_SWIR:long_name = "SWIR Band Quality Flag" ;
                qual_SWIR:flag_masks = 1UB ;
                qual_SWIR:flag_meanings = "saturation" ;
  } // group observation_data
}
```

Appendix B – OCI Calibration LUT

```
netcdf PACE_OCI_L1B_LUT_2024-04_05 {
dimensions:
        blue_bands = 512 ;
        red_bands = 512 ;
        SWIR_bands = 9 ;
        number_of_times = UNLIMITED ; // (27 currently)
        number_of_temperatures = 32 ;
        number_of_CCD_temperatures = 8 ;
        number_of_SWIR_temperatures = 23 ;
        number_of_HAM_sides = 2 ;
        number_of_MCE_sides = 2 ;
        number_of_T_coefficients = 2 ;
        number_of_RVS_coefficients = 4 ;
        number_of_nonlinearity_coefficients = 5 ;
        number_of_polarization_coefficients = 3 ;
        number_of_hysteresis_terms = 4 ;
// global attributes:
                :title = "PACE OCI Radiometric Calibration LUT" ;
                :instrument = "OCI" ;
                :radiance_model = "Lt = K1*K2(t)*(1-K3*(T-Tref))*K4(pixel) *K5(dn)*dn" ;
                :date_created = "2024-04-05T11:32:32Z" ;

group: blue {
  variables:
        float K1(blue_bands, number_of_HAM_sides) ;
                K1:desc = "count to W/(m2*um*sr) [band]" ;
                K1:units = "W/(m2*um*sr)/dn" ;
        float K2(blue_bands, number_of_HAM_sides, number_of_times) ;
                K2:desc = "temporal correction [band,pixel,time]" ;
                K2:units = "unitless" ;
        float K3_coef(blue_bands, number_of_CCD_temperatures, number_of_T_coefficients) ;
                K3_coef:desc = "temperature correction coefficients [band]" ;
                K3_coef:units = "unitless" ;
        float K4_coef(blue_bands, number_of_HAM_sides, number_of_RVS_coefficients) ;
                K4_coef:desc = "RVS polynomial coefficients [band, HAM side]" ;
                K4_coef:units = "unitless" ;
        float K4_sca(blue_bands, number_of_HAM_sides) ;
                K4_sca:desc = "RVS for solar calibrator [band, HAM side]" ;
                K4_sca:units = "unitless" ;
        double K5_coef(blue_bands, number_of_nonlinearity_coefficients) ;
                K5_coef:desc = "nonlinearity of band [band]" ;
                K5_coef:units = "unitless" ;
        int sat_thres(blue_bands) ;
                sat_thres:desc = "saturation threshold (dn)" ;
                sat_thres:units = "counts" ;
        float m12_coef(blue_bands, number_of_HAM_sides, number_of_polarization_coefficients) ;
                m12_coef:desc = "m12_coef/M11 polynomial coefficients (polarization sensitivity, Qt) [band,
HAM side]" ;
                m12_coef:units = "unitless" ;
```

```
        float m13_coef(blue_bands, number_of_HAM_sides, number_of_polarization_coefficients) ;
                m13_coef:desc = "m13_coef/M11 polynomial coefficients (polarization sensitivity, Ut) [band,
HAM side]" ;
                m13_coef:units = "unitless" ;
        float m12_sca(blue_bands, number_of_HAM_sides) ;
                m12_sca:desc = "m12_coef/M11 for solar calibrator (polarization sensitivity, Qt) [band, HAM
side]" ;
                m12_sca:units = "unitless" ;
        float m13_sca(blue_bands, number_of_HAM_sides) ;
                m13_sca:desc = "m13_coef/M11 for solar calibrator (polarization sensitivity, Ut) [band, HAM
side]" ;
                m13_sca:units = "unitless" ;
 } // group blue

group: red {
 variables:
        float K1(red_bands, number_of_HAM_sides) ;
                K1:desc = "count to W/(m2*um*sr) [band]" ;
                K1:units = "W/(m2*um*sr)/dn" ;
        float K2(red_bands, number_of_HAM_sides, number_of_times) ;
                K2:desc = "temporal correction [band,pixel,time]" ;
                K2:units = "unitless" ;
        float K3_coef(red_bands, number_of_CCD_temperatures, number_of_T_coefficients) ;
                K3_coef:desc = "temperature correction coefficients [band]" ;
                K3_coef:units = "unitless" ;
        float K4_coef(red_bands, number_of_HAM_sides, number_of_RVS_coefficients) ;
                K4_coef:desc = "RVS polynomial coefficients [band, HAM side]" ;
                K4_coef:units = "unitless" ;
        float K4_sca(red_bands, number_of_HAM_sides) ;
                K4_sca:desc = "RVS for solar calibrator [band, HAM side]" ;
                K4_sca:units = "unitless" ;
        double K5_coef(red_bands, number_of_nonlinearity_coefficients) ;
                K5_coef:desc = "nonlinearity of band [band]" ;
                K5_coef:units = "unitless" ;
        int sat_thres(red_bands) ;
                sat_thres:desc = "saturation threshold (dn)" ;
                sat_thres:units = "counts" ;
        float m12_coef(red_bands, number_of_HAM_sides, number_of_polarization_coefficients) ;
                m12_coef:desc = "m12_coef/M11 polynomial coefficients (polarization sensitivity, Qt) [band,
HAM side]" ;
                m12_coef:units = "unitless" ;
        float m13_coef(red_bands, number_of_HAM_sides, number_of_polarization_coefficients) ;
                m13_coef:desc = "m13_coef/M11 polynomial coefficients (polarization sensitivity, Ut) [band,
HAM side]" ;
                m13_coef:units = "unitless" ;
        float m12_sca(red_bands, number_of_HAM_sides) ;
                m12_sca:desc = "m12_coef/M11 for solar calibrator (polarization sensitivity, Qt) [band, HAM
side]" ;
                m12_sca:units = "unitless" ;
        float m13_sca(red_bands, number_of_HAM_sides) ;
                m13_sca:desc = "m13_coef/M11 for solar calibrator (polarization sensitivity, Ut) [band, HAM
side]" ;
                m13_sca:units = "unitless" ;
```

```
 } // group red

group: SWIR {
 variables:
        float K1(SWIR_bands, number_of_HAM_sides) ;
                K1:desc = "count to W/(m2*um*sr) [band]" ;
                K1:units = "W/(m2*um*sr)/dn" ;
        float K2(SWIR_bands, number_of_HAM_sides, number_of_times) ;
                K2:desc = "temporal correction [band,pixel,time]" ;
                K2:units = "unitless" ;
        float K3_coef(SWIR_bands, number_of_SWIR_temperatures, number_of_T_coefficients) ;
                K3_coef:desc = "temperature correction coefficients [band]" ;
                K3_coef:units = "unitless" ;
        float K4_coef(SWIR_bands, number_of_HAM_sides, number_of_MCE_sides,
number_of_RVS_coefficients) ;
                K4_coef:desc = "RVS polynomial coefficients [band, HAM side]" ;
                K4_coef:units = "unitless" ;
        float K4_sca(SWIR_bands, number_of_HAM_sides, number_of_MCE_sides) ;
                K4_sca:desc = "RVS for solar calibrator [band, HAM side]" ;
                K4_sca:units = "unitless" ;
        double K5_coef(SWIR_bands, number_of_nonlinearity_coefficients) ;
                K5_coef:desc = "nonlinearity of band [band]" ;
                K5_coef:units = "unitless" ;
        int sat_thres(SWIR_bands) ;
                sat_thres:desc = "saturation threshold (DN)" ;
                sat_thres:units = "counts" ;
        float hyst_time_const(SWIR_bands, number_of_hysteresis_terms) ;
                hyst_time_const:desc = "time constants of hysteresis corrections" ;
                hyst_time_const:units = "science pixels" ;
        float hyst_amplitude(SWIR_bands, number_of_hysteresis_terms) ;
                hyst_amplitude:desc = "amplitudes of hysteresis corrections" ;
                hyst_amplitude:units = "unitless" ;
        float m12_coef(SWIR_bands, number_of_HAM_sides, number_of_polarization_coefficients) ;
                m12_coef:desc = "m12_coef/M11 polynomial coefficients (polarization sensitivity, Qt) [band,
HAM side]" ;
                m12_coef:units = "unitless" ;
        float m13_coef(SWIR_bands, number_of_HAM_sides, number_of_polarization_coefficients) ;
                m13_coef:desc = "m13_coef/M11 polynomial coefficients (polarization sensitivity, Ut) [band,
HAM side]" ;
                m13_coef:units = "unitless" ;
        float m12_sca(SWIR_bands, number_of_HAM_sides) ;
                m12_sca:desc = "m12_coef/M11 for solar calibrator (polarization sensitivity, Qt) [band, HAM
side]" ;
                m12_sca:units = "unitless" ;
        float m13_sca(SWIR_bands, number_of_HAM_sides) ;
                m13_sca:desc = "m13_coef/M11 for solar calibrator (polarization sensitivity, Ut) [band, HAM
side]" ;
                m13_sca:units = "unitless" ;
 } // group SWIR
```

```
group: common {
  variables:
        float blue_wavelength(blue_bands) ;
                blue_wavelength:_FillValue = -32767.f ;
                blue_wavelength:long_name = "Band center wavelengths for bands from blue CCD" ;
                blue_wavelength:valid_min = 305.f ;
                blue_wavelength:valid_max = 610.f ;
                blue_wavelength:units = "nm" ;
        float red_wavelength(red_bands) ;
                red_wavelength:_FillValue = -32767.f ;
                red_wavelength:long_name = "Band center wavelengths for bands from red CCD" ;
                red_wavelength:valid_min = 590.f ;
                red_wavelength:valid_max = 900.f ;
                red_wavelength:units = "nm" ;
        float SWIR_wavelength(SWIR_bands) ;
                SWIR_wavelength:_FillValue = -32767.f ;
                SWIR_wavelength:long_name = "Band center wavelengths for SWIR bands" ;
                SWIR_wavelength:valid_min = 939.f ;
                SWIR_wavelength:valid_max = 2261.f ;
                SWIR_wavelength:units = "nm" ;
        float blue_F0(blue_bands) ;
                blue_F0:_FillValue = -32767.f ;
                blue_F0:long_name = "Solar irradiance for bands from blue CCD" ;
                blue_F0:units = "W/(m2*um)" ;
        float red_F0(red_bands) ;
                red_F0:_FillValue = -32767.f ;
                red_F0:long_name = "Solar irradiance for bands from red CCD" ;
                red_F0:units = "W/(m2*um)" ;
        float SWIR_F0(SWIR_bands) ;
                SWIR_F0:_FillValue = -32767.f ;
                SWIR_F0:long_name = "Solar irradiance for SWIR bands" ;
                SWIR_F0:units = "W/(m2*um)" ;
        double K2t(number_of_times) ;
                K2t:desc = "time reference, days since 2000-01-01" ;
                K2t:units = "days" ;
        float K3T(number_of_temperatures) ;
                K3T:desc = "temperature reference, C [temperature]" ;
                K3T:units = "degree (C)" ;
  } // group common
}
```

Appendix C – OCI Geolocation LUT

```
netcdf example_OCI_GEO_LUT {
dimensions:
        number_of_HAM_sides = 2 ;
        number_of_tilts = 2 ;
        number_of_mce_boards = 2 ;
        vector_size = 3 ;
        planarity_coefficients = 5;
// global attributes:
                :title = "PACE OCI Geolocation LUT" ;
                :instrument = "OCI" ;
                :date_created = "2024-04-30T16:00:00Z" ;
                :reference = "" ;

group: time_params {
  variables:
        double master_clock ;
                master_clock:units = "Hz" ;
                master_clock:desc = "Frequency of OCI master clock" ;
        double MCE_clock ;
                MCE_clock:units = "Hz" ;
                MCE_clock:desc = "Frequency of OCI MCE clock" ;
  } // group time_params

group: coord_trans {
  variables:
        double sc_to_tilt (vector_size, vector_size) ;
                sc_to_tilt:desc = "Spacecraft to tilt base transformation" ;
        double tilt_axis (vector_size) ;
                tilt_axis:desc = "Tilt axis in tilt reference frame" ;
        double tilt_angles (number_of_tilts) ;
                tilt_angles:units = "degrees" ;
                tilt_angles:desc = "Tilt angles at fixed positions (aft, forward)" ;
        double   tilt_home ;
                tilt_home:units = "degrees" ;
                tilt_home:desc = "Tilt angle corresponding to mechanism home position" ;
        double tilt_to_oci_mech (vector_size, vector_size) ;
                tilt_to_oci_mech:desc = "Tilt platform to OCI mechanical transformation" ;
        double oci_mech_to_oci_opt (vector_size, vector_size) ;
                oci_mech_to_oci_opt:desc = "OCI mechanical to optical transformation" ;
  } // group coord_trans

group: RTA_HAM_params {
  variables:
        double HAM_AT_angles (number_of_HAM_sides) ;
                HAM_AT_angles:desc = "HAM along-track mirror angles to axis" ;
                HAM_AT_angles:units = "arcseconds" ;
        double HAM_CT_angles (number_of_HAM_sides) ;
                HAM_CT_angles:desc = "HAM cross-track mirror angles to axis" ;
                HAM_CT_angles:units = "arcseconds" ;
        double RTA_enc_scale ;
                RTA_enc_scale:desc = "RTA encoder conversion to arcseconds" ;
```

```
                RTA_enc_scale:units = "arcseconds" ;
        double HAM_enc_scale ;
                HAM_enc_scale:desc = "HAM encoder conversion to arcseconds" ;
                HAM_enc_scale:units = "arcseconds" ;
        long RTA_nadir (number_of_mce_boards) ;
                RTA_nadir:desc = "PPR offset from RTA nadir angle in encoder counts" ;
  } // group RTA_HAM_params

group: planarity {
  variables:
        double along_scan_planarity (planarity_coefficients) ;
                along_scan_planarity:desc = "Along-scan deviation from ideal scan" ;
                along_scan_planarity:units = "arcseconds" ;
        double along_track_planarity (planarity_coefficients) ;
                along_track_planarity:desc = "Along-track deviation from ideal scan" ;
                along_track_planarity:units = "arcseconds" ;
  } // group planarity

}
```

Previous Volumes in This Series

Volume 1 *April 2018*	ACE Ocean Working Group recommendations and instrument requirements for an advanced ocean ecology mission
Volume 2 *May 2018*	Pre-Aerosol, Clouds, and ocean Ecosystem (PACE) Mission Science Definition Team Report
Volume 3 *October 2018*	Polarimetry in the PACE mission: Science Team consensus document
Volume 4 *October 2018*	Cloud retrievals in the PACE mission: Science Team consensus document
Volume 5 *December 2018*	Mission Formulation Studies
Volume 6 *December 2018*	Data Product Requirements and Error Budgets
Volume 7 *December 2018*	Ocean Color Instrument (OCI) Concept Design Studies
Volume 8 *September 2020*	The PACE Science Data Product Selection Plan
Volume 9 *October 2020*	PACE Application Plan
Volume 10 *March 2022*	ACE Ocean Product Accuracy Assessments: A record of the state of the art circa 2010
Volume 11 *June 2023*	The PACE Postlaunch Airborne eXperiment (PACE-PAX)
Volume 12 *March 2024*	The PACE Level 1C data format